# 1.1-billion-year-old porphyrins establish a marine ecosystem dominated by bacterial primary producers

N. Gueneli[a,1], A. M. McKenna[b], N. Ohkouchi[c], C. J. Boreham[d], J. Beghin[e], E. J. Javaux[e], and J. J. Brocks[a,1]

[a]Research School of Earth Sciences, Australian National University, Canberra, ACT 2601, Australia; [b]National High Magnetic Field Laboratory, Florida State University, Tallahassee, FL 32310-4005; [c]Department of Biogeochemistry, Japan Agency for Marine–Earth Science and Technology, 237-0061 Kanagawa Prefecture, Yokosuka, Natsushimacho, Japan; [d]Geoscience Australia, Symonston, ACT 2609, Australia; and [e]Department of Geology, Unité de Recherche Geology, University of Liège, 4000 Liege, Belgium

Edited by Andrew H. Knoll, Harvard University, Cambridge, MA, and approved June 8, 2018 (received for review March 6, 2018)

**The average cell size of marine phytoplankton is critical for the flow of energy and nutrients from the base of the food web to higher trophic levels. Thus, the evolutionary succession of primary producers through Earth's history is important for our understanding of the radiation of modern protists ∼800 million years ago and the emergence of eumetazoan animals ∼200 million years later. Currently, it is difficult to establish connections between primary production and the proliferation of large and complex organisms because the mid-Proterozoic (∼1,800–800 million years ago) rock record is nearly devoid of recognizable phytoplankton fossils. We report the discovery of intact porphyrins, the molecular fossils of chlorophylls, from 1,100-million-year-old marine black shales of the Taoudeni Basin (Mauritania), 600 million years older than previous findings. The porphyrin nitrogen isotopes ($\delta^{15}N_{por}$ = 5.6–10.2‰) are heavier than in younger sedimentary sequences, and the isotopic offset between sedimentary bulk nitrogen and porphyrins ($\varepsilon_{por}$ = −5.1 to −0.5‰) points to cyanobacteria as dominant primary producers. Based on fossil carotenoids, anoxygenic green (Chlorobiacea) and purple sulfur bacteria (Chromatiaceae) also contributed to photosynthate. The low $\varepsilon_{por}$ values, in combination with a lack of diagnostic eukaryotic steranes in the time interval of 1,600–1,000 million years ago, demonstrate that algae played an insignificant role in mid-Proterozoic oceans. The paucity of algae and the small cell size of bacterial phytoplankton may have curtailed the flow of energy to higher trophic levels, potentially contributing to a diminished evolutionary pace toward complex eukaryotic ecosystems and large and active organisms.**

chlorophyll | Taoudeni Basin | Mesoproterozoic | compound-specific nitrogen isotopes | primary producers

The succession of primary producers in the oceans shaped marine ecology through Earth's history (1). Primary producers form the base of the food web. Their cell size, elemental stoichiometry, and cell density influence the flow of energy and nutrients to higher trophic levels (2), presumably setting limits for ecosystem complexity. The composition of phytoplankton communities in Earth's early oceans, including anoxygenic and oxygenic phototrophic bacteria and eukaryotic algae, may thus have set the pace for the emergence and radiation of different groups of filter feeders, grazers, and predators, including the proliferation of modern protists ∼800 Ma and the appearance of eumetazoan animals some 200 My later (1) (Fig. 1*B*).

Based on the fossil record, chlorophyll *c* (Chl *c*) algae, including dinoflagellates, coccolithophorids, and diatoms, were the major energy and carbon source in the oceans of the past ∼250 My (Fig. 1*B*). By contrast, Paleozoic (541–251 Ma) and Ediacaran (635–541 Ma) oceans were presumably dominated by primary endosymbiotic algae (Archaeplastida), encompassing the red (Rhodophyta) and green algae (Chlorophyta) (1). Deeper yet in time, reconstructing the succession of primary producers becomes challenging. Phytoplankton without a preservable cuticle or skeleton are rarely preserved in the body fossil record, and there are no uncontentious fossils of planktonic bacteria or algae in the pre-Ediacaran (3). However, biomarkers, the molecular fossils of biological lipids, can provide complementary information about primary producers. For example, hydrocarbon fossils of carotenoid pigments extracted from sedimentary rocks have been used to detect phototrophic green (Chlorobiaceae) and purple sulfur bacteria (PSB) (Chromatiaceae) in 1,640-My-old marine ecosystems (4, 5), while the concentration of eukaryotic steranes, relative to bacterial hopanes, may provide basic information about the ecological relevance of Precambrian algae (6). The relative abundance as well as diversity of steranes dramatically increased in the brief interlude between the Sturtian and Marinoan snowball Earth glaciations of 659–645 Ma, heralding the rise of planktonic algae as important primary producers in the oceans (Fig. 1*A*). Steranes in the time interval 645 to ∼500 Ma have a strong predominance of stigmastane (a structure with 29 carbon atoms, $C_{29}$), revealing Chlorophyta, a division of green algae, as dominant primary producers from the late Cryogenian to early Paleozoic (Fig. 1) (7, 8).

Preceding the Cryogenian rise of planktonic algae, the oldest clearly indigenous eukaryotic steranes appear in the geological record ∼900–800 Ma, albeit in low concentrations relative to bacterial biomarkers (7, 8). These Tonian (1,000–720 Ma) steranes display a primordial distribution with a nearly 100% predominance of cholestane ($C_{27}$, red circles in Fig. 1*A*), which may be related to the activity of rhodophytes (9) or heterotrophic eukaryotes (8).

## Significance

**The oceans of Earth's middle age, 1.8–0.8 billion years ago, were devoid of animal-like life. According to one hypothesis, the emergence of large, active organisms was restrained by the limited supply of large food particles such as algae. Through the discovery of molecular fossils of the photopigment chlorophyll in 1.1-billion-year-old marine sedimentary rocks, we were able to quantify the abundance of different phototrophs. The nitrogen isotopic values of the fossil pigments showed that the oceans were dominated by cyanobacteria, while larger planktonic algae were scarce. This supports the hypothesis that small cells at the base of the food chain limited the flow of energy to higher trophic levels, potentially retarding the emergence of large and complex life.**

Author contributions: N.G. and J.J.B. designed research; N.G., A.M.M., N.O., C.J.B., and J.J.B. performed research; A.M.M., N.O., and C.J.B. contributed new reagents/analytic tools; N.G., A.M.M., N.O., C.J.B., and J.J.B. analyzed data; and N.G., A.M.M., N.O., J.B., E.J.J., and J.J.B. wrote the paper.

The authors declare no conflict of interest.

This article is a PNAS Direct Submission.



[1]To whom correspondence may be addressed. Email: nur.gueneli@anu.edu.au or jochen.brocks@anu.edu.au.

This article contains supporting information online at www.pnas.org/lookup/suppl/doi:10.1073/pnas.1803866115/-/DCSupplemental.

Published online July 9, 2018.

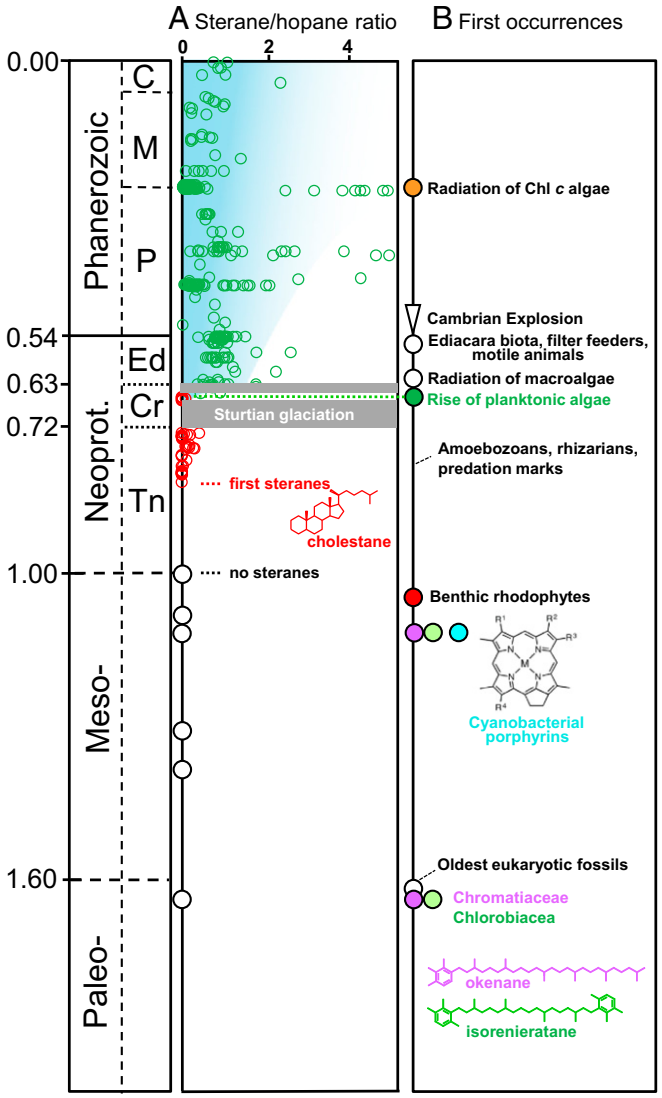


**Fig. 1.** Temporal history of biomarker and fossil data. (*A*) Ratio of eukaryotic steranes over bacterial hopanes through time (details and references see text). Green circles, late Cryogenian to present data, including $C_{27}$ to $C_{29}$ steranes (cholestanes, ergostanes, and stigmastanes); red circles, Tonian to early Cryogenian steranes with a ∼100% cholestane predominance; and unfilled black circles, mid-Proterozoic biomarker assemblages, where hopanes are present but steranes are below detection limits. (*B*) First occurrences or radiations of organism groups and biomarkers (for data sources, see text). C, Cenozoic; Cr, Cryogenian; Ed, Ediacaran; M, Mesozoic; Neoprot., Neoproterozoic; P, Paleozoic; Tn, Tonian.

Going yet further back in time into the mid-Proterozoic (1,800–800 Ma), evidence for algae becomes scarce. Based on molecular clocks, the last common ancestor of all algae originated broadly between 1,900 and 1,400 Ma (10, 11), predating the oldest unambiguous fossil of a eukaryotic phototroph, the ∼1,050 Ma (12) benthic red alga *Bangiomorpha* (13) (Fig. 1*B*). However, clearly indigenous biomarkers for algae have not yet been found in sedimentary rocks >900 Ma despite preservation of bacterial hopanes (Fig. 1). Whether this lack of steranes is caused by preferential degradation of algal organic matter (14) or reflects genuine paucity of eukaryotic phototrophs, remains unresolved.

Here, we present an approach to gauge the activity of bacterial and eukaryotic primary producers in the Precambrian. Based on Fourier transform ion cyclotron resonance mass spectrometry (FT-ICR MS), we identify geoporphyrins in 1,100-My-old black shales. Porphyrins are the molecular fossils of (bacterio)chlorophylls. Their nitrogen isotopic composition can provide quantitative information about dominant phototrophs in past ecosystems (15). Some groups of phototrophs possess a characteristic offset ($\varepsilon_{por}$) between the nitrogen isotopic composition of the whole cell and chlorophylls, independent of the nitrogen source (15), and under suitable conditions this isotopic offset is largely unaffected by degradation processes in the water column and bottom sediments (16). Therefore, the nitrogen isotopic composition of porphyrins in sediments and sedimentary rocks may preserve information about primary producers present in an ancient environment, largely independent of physical and chemical conditions such as food source and diagenesis.

## Depositional Environment

Eleven black shales studied for their molecular content (Table 1 and *SI Appendix*, Table S1) come from the En Nesoar and Touirist formations of the 1,100 Ma El Mreïti Group (17) deposited on an epicratonic platform of the Taoudeni Basin on the West African Craton (18). The black shales, with a carbon content of up to 32%, accumulated beneath anoxic ferruginous and occasionally sulfidic waters (19) during maximal flooding of the craton in a quiet subwave base environment possibly protected by offshore stromatolite reefs (18). The black shales contain micrometer-thin laminae of organic matter and pyritized filamentous sheaths that are interpreted as benthic microbial communities, presumably of heterotrophic and/or chemosynthetic microorganisms thriving beneath anoxic waters (19), and irregularly shaped, discrete or bedding-parallel accumulations of organic particles typical of planktonic debris (*SI Appendix*, *SI Geology and Samples*).

## Results

**Biomarker Syngeneity.** Potential contaminants introduced in the laboratory were monitored using comprehensive accumulatory system blanks, and compounds that may have permeated into rock samples were quantified and eliminated by comparing the concentration of individual hydrocarbons in the exterior and interior portions of the rock (20–22). All compounds reported here are demonstrably indigenous (*SI Appendix*, *SI Syngeneity Assessment*).

**Hydrocarbon Biomarkers.** All El Mreïti Group shales yielded pentacyclic terpanes, including αβ-hopanes with 27–35 carbon atoms as well as gammacerane (Fig. 2*A*). A complete series of $C_{31}$ to $C_{36}$ 2α-methylhopanes was also present in low concentrations. The 2α-methylhopane index, defined as the abundance of $C_{31}$ 2α-methylhopane relative to $C_{30}$ αβ-hopane, was low, ranging between 0.35 and 0.77%. Although hopanes were well above detection limits, $C_{26}$ to $C_{30}$ steranes were not detected in any sample (Table 1 and *SI Appendix*, Fig. S1), consistent with a previous study on Atar Group shales that also failed to detect steranes (23). Based on determination of detection limits, the maximum level of steranes that may be present beneath the noise is extremely low. The ratio of maximum hypothetical $C_{27}$ steranes relative to $C_{27–35}$ hopanes ($S/H_{max}$) falls into the range of 0.0002–0.0014 (average, 0.00065; $n = 11$; Table 1). The El Mreïti Group shales were also devoid of the saturated carotenoid derivatives lycopane, β-carotane and γ-carotane. However, two of the most dominant biomarker classes in the aromatic hydrocarbon fraction were $C_{13}$ to $C_{27}$ 2,3,6-trimethyl aryl isoprenoids (2,3,6-AI) and $C_{13}$ to $C_{30}$ 2,3,4-trimethyl aryl isoprenoids (2,3,4-AI) (Fig. 2*B*), the degradation products of aromatic carotenoids.

**Identification of Porphyrins.** Geoporphyrins were identified using reversed-phase HPLC-UV/Vis and atmospheric pressure photoionization coupled to FT-ICR MS at 9.4 tesla. Based on HPLC

**Table 1. Bulk and biomarker data for Mesoproterozoic shales of the El Mreïti Group, Taoudeni Basin, from drill core S2**

| | Sample ID | | | | | | | | | | |
|---|---|---|---|---|---|---|---|---|---|---|---|
| Specs | 06 | 08 | 11 | 13 | 14 | 17 | 20 | 22 | 29 | 32 | 33 |
| Formation | Touirist | Touirist | Touirist | Touirist | Touirist | Touirist | En Nesoar | En Nesoar | En Nesoar | En Nesoar | En Nesoar |
| Depth | 139.60 | 140.25 | 140.55 | 141.90 | 142.20 | 151.95 | 185.40 | 187.30 | 200.01 | 203.10 | 206.08 |
| TOC, wt % | 10.0 | 16.5 | 16.2 | 31.7 | 15.9 | 15.8 | 2.1 | 11.1 | 12.6 | 14.8 | 8.5 |
| $N_{bulk}$, wt % | 0.3 | N.A. | 0.5 | 0.7 | 0.5 | 0.5 | 0.1 | 0.3 | 0.3 | 0.3 | 0.2 |
| $\delta^{13}C_{org}$, ‰ | −31.5 | N.A. | −31.2 | −33.9 | −31.2 | −31.7 | −31.7 | −32.5 | −34.9 | −34.3 | −35.5 |
| $\delta^{15}N_{bulk}$, ‰ | 4.4 | N.A. | 4.7 | 5.1 | 5.1 | 4.2 | 4.6 | 5.0 | 6.1 | 6.1 | 6.0 |
| $S/H_{max}$* | 0.0002 | 0.0004 | 0.0002 | 0.0004 | 0.0006 | 0.0004 | 0.0014 | 0.0006 | 0.0011 | 0.0008 | 0.0011 |

N.A., not available; TOC, total organic carbon.

*Steranes (S) were beneath detection limits in all samples. The $S/H_{max}$ ratio gives the maximum concentration of $C_{27}$ steranes relative to bacterial $C_{27}$ to $C_{35}$ hopanes (H) that may be present in samples beneath the analytical noise (*SI Appendix, SI Methods*).

coinjection with porphyrin standards and comparison with reference material (24, 25) (*SI Appendix*, Fig. S2), the most abundant porphyrins are nickel Etio porphyrins (**1**), $C_{30}$ to $C_{32}$ deoxophylloerythroetioporphyrins (DPEP, **2a–f**), $C_{31}$ and $C_{32}$ butano (**3a-b**), and $C_{34}$ diDPEP (**4a**) porphyrins, as well as tentatively identified vanadyl (VO) $C_{30}$-$C_{32}$ DPEP (**2a,b,f**) (structure numbers are defined in Fig. 3). FT-ICR MS isoabundance-contoured plots confirm $C_{29}$ to $C_{32}$ DPEP (**2**) and $C_{29}$ to $C_{31}$ Etio (**1**) as the most abundant Ni-porphyrins, and $C_{32}$ DPEP and $C_{30}$ Etio as the highest concentrated VO-porphyrin (Fig. 4). Also identified were Ni- and VO-based di-DPEP (**4**, **5**, and/or **6**), rhodo-Etio (**7**), and rhodo-DPEP (**8**) (26). Each of these compound classes occurs as homologous series across a wide carbon number distribution with more than 40 carbon atoms (Fig. 4*A*) due to side-chain length variation off core structural motifs. Although these side-chain elongated porphyrins may include bacteriochlorophyll (BChl)-derived structures (27), sample limitation prevented characterization of precise alkyl side-chain configurations (*SI Appendix*, *SI Additional Details on Biomarker Identification and Interpretation*).

**Nitrogen and Carbon Isotopic Composition of Individual Ni-Porphyrins.** For the richest sample (#13), it was possible to measure the carbon and nitrogen isotopic compositions of six isolated and purified Ni-porphyrins (*SI Appendix*, Fig. S3*G*). Based on molecular masses for isolated compounds determined by HPLC–atmospheric pressure chemical ionization (APCI)–MS, purified porphyrins correspond to $C_{28}$ to $C_{31}$ Etio and $C_{30}$ and $C_{32}$ DPEP structures (Table 2). Measured C/N ratios of the purified porphyrins (C/N = 12.7–22.1) were higher than predicted stoichiometries (C/N = 7.0–8.0; Table 2), which suggests that isolates still contained other nonporphyrin compounds that were carried over across multiple steps of chromatographic purification (*SI Appendix*, Fig. S4). However, the APCI mass spectra of the isolated fractions (*SI Appendix*, Fig. S3 *A–F*) all show relatively clean molecular ions diagnostic for individual Ni-porphyrins and only minor foreign masses. This indicates that the contaminants are poorly ionized by APCI and likely represent hydrocarbons. The presence of nonporphyrinic nitrogen-containing compounds is unlikely in these fractions due to their higher polarity relative to porphyrins and absence of significant signals in the APCI mass spectra (see *SI Appendix*, *SI Methods* for a detailed discussion about avoidance of artifacts and contaminants). The $\delta^{15}N_{por}$ values measured for six porphyrins ranged between 5.6‰ and 10.2‰, with corresponding values of $\varepsilon_{por}$ between −0.5 and −5.1‰ (Table 2).

## Discussion

**Bulk Nitrogen Isotopes.** The bulk-rock nitrogen isotopic composition ($\delta^{15}N_{bulk}$) of the En Nesoar and Touirist Formation shales falls into the narrow range of 4.2–6.1‰ ($n$ = 11, average = 5.1‰, Table 1) and is slightly higher than those of the Mesoproterozoic Belt Basin (−1.1–5.2‰) (28). Although $\delta^{15}N_{bulk}$ of organic-rich shales, such as those studied here with total organic carbon (TOC) between 2.1 and 31.7%, commonly closely reflect the nitrogen isotopic composition of primary bulk organic matter (29), two factors must be considered before interpreting the data: first, the contribution of inorganic nitrogen to $\delta^{15}N_{bulk}$ values, and second, isotopic fractionation effects associated with diagenesis and heterotrophic reworking of photosynthate.

Although inorganic nitrogen sources are usually negligible in organic matter-rich samples (16), the El Mreïti Group shales may contain up to 0.1% inorganic nitrogen (see intercept on $N_{bulk}$ axis in *SI Appendix*, Fig. S5) (30). However, it is plausible that the conversion of smectite to illite during burial diagenesis of the clay-rich

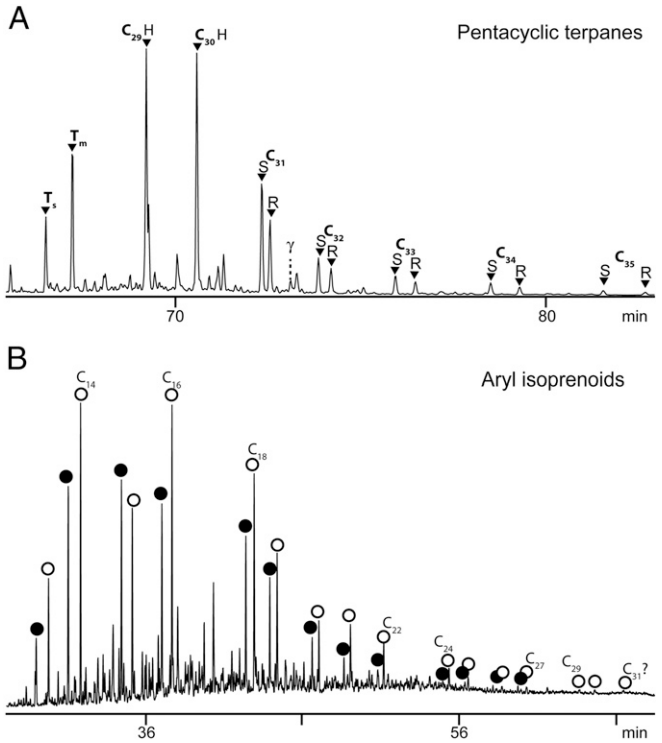


**Fig. 2.** Selected biomarker classes identified in black shales (sample 08, drill core S2, 140.25 m) of the El Mreïti Group. (*A*) Summed GC-MS metastable reaction monitoring (MRM) chromatograms of M+ → 191 transitions of the saturated fraction. A complete homologous series of 17α(*H*),21β(*H*)-hopanes with 27–35 carbon atoms (black triangles) were identified. $T_s$ = 18α(*H*)-22,29,30 trisnorneohopane, $T_m$ = 17α(H)-22,29,30-trisnorhopane, and γ = gammacerane. (*B*) *m/z* 134 selected ion recording chromatogram of the aromatic fraction. Filled circles, 2,3,6-AI; open circles, 2,3,4-AI.

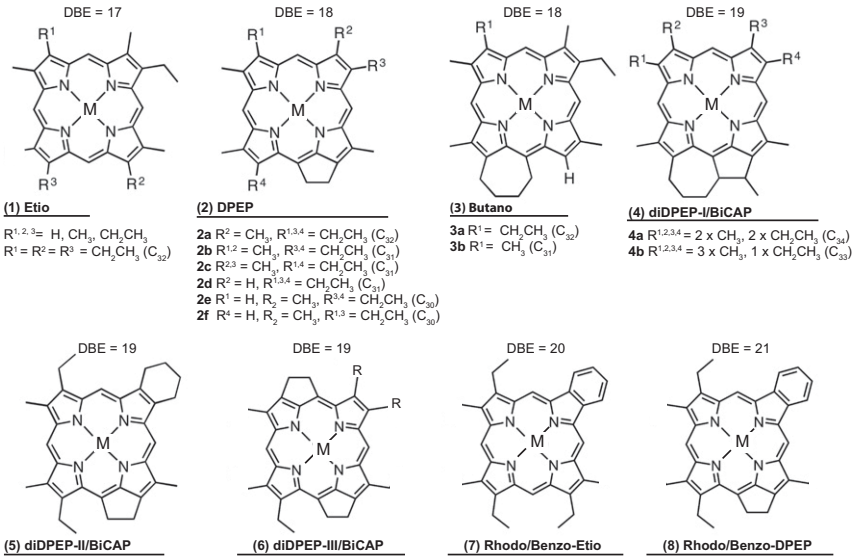


**Fig. 3.** Structures of nickel and vanadyl-oxide porphyrins discussed in the text. M, Ni, or VO. DBE, double bond equivalents (i.e., number of rings plus double bonds).

samples yielded substitution of potassium by ammonium (e.g., ref. 31). As the ammonium would have largely derived from the decomposition of organic matter, and as the substitution process is not coupled to major isotopic fractionation (32), $\delta^{15}N_{bulk}$ probably largely reflects the nitrogen isotopic composition of the organic matter. This is further confirmed by the absence of a correlation between TOC and $\delta^{15}N_{bulk}$.

Secondary processes in the water column or bottom sediment may alter the original N-isotopic composition of the primary organic matter. In modern environments, aerobic heterotrophic reworking of primary organic matter in marine regions with low organic carbon flux and high oxygen exposure times increases $\delta^{15}N_{bulk}$ by +3 to +5‰ (33). However, $\delta^{15}N_{bulk}$ values of high TOC sediments do not have such positive isotopic offsets and faithfully record the N-isotopic composition of primary producers (29). Conversely, in anaerobic waters, $\delta^{15}N_{bulk}$ may decrease by 3‰ under laboratory conditions, and a depletion of 1.2‰ has been observed in anoxic sediments of Lake Lugano (34). However, in two large modern anoxic marine basins, the Black Sea and the Cariaco Trench, no negative N-isotopic offsets were observed (35, 36). Moreover, a study of Black Sea sediments found that the isotopic difference between $\delta^{15}N_{bulk}$ and $\delta^{15}N_{por}$ faithfully records $\varepsilon_{por}$ of phytoplankton (16). Thus, $\delta^{15}N_{bulk}$ of modern organic-rich shales likely reflect $\delta^{15}N$ of contemporaneous phytoplankton.

Our data extend the record of $\varepsilon_{por}$, the offset between $\delta^{15}N_{bulk}$ and $\delta^{15}N_{por}$, by nearly 1 Gy. Problems associated with the extrapolation of nitrogen isotopic information over such immense periods of time, into an eon with potentially different degradation processes, are discussed in detail in *SI Appendix*, *SI Taphonomic Biases*. However, even taking possible nonuniformitarian processes into account, it is likely that $\varepsilon_{por}$ of highly organic-rich Proterozoic shales, such as those studied here, reflect the nitrogen isotopic composition of primary biomass. Moreover, even large alterations of $\delta^{15}N_{bulk}$ in the range of −3‰ to +10‰ would not impact our conclusions.

**Porphyrin Nitrogen Isotopes ($\delta^{15}N_{por}$).** The measured $\delta^{15}N$ values of porphyrins ($\delta^{15}N_{por}$) range between +5.6‰ and +10.2‰ and are at the isotopically heavy end of data observed in modern and Phanerozoic (541 Ga to present) aquatic systems (Fig. 5). Geoporphyrins are believed to reflect the nitrogen isotopic composition of the precursor chlorophylls ($\delta^{15}N_{Chl}$). For example, the isotopic offset between total organic matter and porphyrins remains largely constant during burial (16), and demetallation and metal-complex formation during chlorophyll diagenesis have commonly very little effect on nitrogen isotopic fractionation (37). Thus, the isotopic composition of the Mesoproterozoic geoporphyrins likely represent $\delta^{15}N$ of the precursor (bacterio) chlorophylls (*SI Appendix*, *SI Taphonomic Biases*).

**Biological Origins of the Geoporphyrins.** The previously oldest geoporphyrins come from the early Cambrian (38), so the structures reported here extend the record by 600 My (*SI Appendix*, *SI Other Reports on Proterozoic Porphyrins*). However, the structures of the 1,100 Ma porphyrins, when viewed in isolation, provide limited biological information. The major (bacterio) chlorophylls and their most important biogenic sources are summarized in *SI Appendix*, Table S2. General evidence for photosynthetic activity in the Taoudeni Basin is provided by $C_{30}$ to $C_{32}$ DPEP (**2**), which may originate from Chl *a*, *b*, and *c*, and BChl *a*, *b*, and *d* (39). More specifically, 7-nor DPEP (**2d**) may originate from Chl *b* and Chl $c_3$ (40, 41), and 17-nor DPEP (**2f**) from Chl *c* (42). Chl *b* is an accessory pigment in higher plants, green algae, and cyanobacteria (43), although it can also be chemically generated by alteration of Chl *a* (44), while Chl *c* is found in chromophyte algae and cyanobacteria (45). Furthermore, the etio (**1**), butano (**3**), diDPEP (**4**, **5**, **6**), and rhodo-structures (**7**, **8**) may have the same biogenic sources as the corresponding DPEP compounds. Hence, the identified porphyrins do not point to any specific chloropigment source and may derive from most groups of oxygenic phototrophs plus a possible contribution from anoxygenic phototrophic bacteria.

More information can be obtained from the nitrogen isotopic composition of the porphyrins. Phototrophic organisms have a specific nitrogen isotopic offset ($\varepsilon_{por}$) between total biomass and chloropigments ($\varepsilon_{por} = \delta^{15}N_{biomass} - \delta^{15}N_{Chl}$) (Fig. 6). In culture experiments, freshwater and marine cyanobacteria, purple nonsulfur bacteria, and green and red algae were grown on different nitrogen sources (15). Despite a wide range of nitrogen isotopic compositions of bulk organic matter ($\delta^{15}N_{bulk}$ = −20 to +20‰) and (bacterio)chlorophylls ($\delta^{15}N_{Chl}$ = −30 to +25‰; *SI Appendix*, Fig. S6), the isotopic offset $\varepsilon_{por}$ is quite uniform within the same group of organisms but relatively distinct between groups. $\varepsilon_{por}$ reflects the difference in nitrogen isotopic fractionation

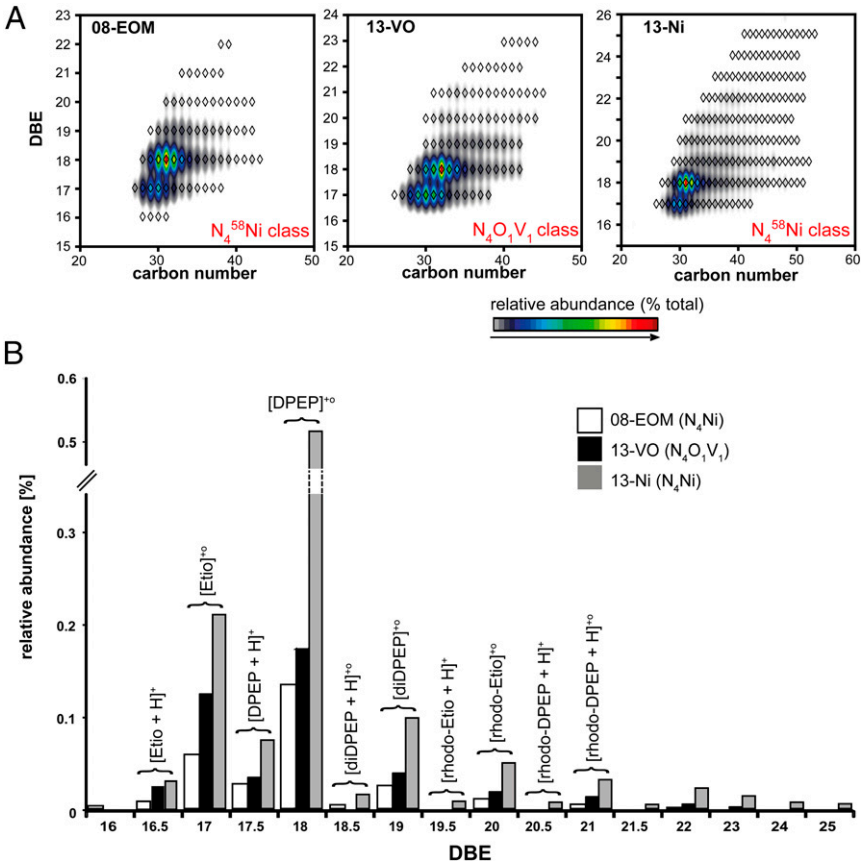


**Fig. 4.** Identification of Ni- and VO-porphyrins by FT-ICR MS. (*A*) Isoabundance-contoured plots of double-bond equivalents (DBEs) versus carbon number for the $N_4{}^{58}Ni$ class (08-EOM and 13-Ni) and the $N_4O_1V_1$ class (13-VO). (*B*) DBE distributions for Ni- and VO-porphyrins in samples 08-EOM, 13-VO, and 13-Ni. Normalized abundances are reported for each sample. Note that $M^{+o}$ and $[M + H]^+$ ions can be distinguished by their integer versus half-integer calculated DBE values.

between chlorophyll biosynthesis and the synthesis of the bulk of other nitrogen-containing metabolites, mainly proteins (16). Furthermore, $\varepsilon_{por}$ is independent of the nitrogen source ($NH_4^+$, $N_2$, or $NO_3^-$) and its isotopic composition (15). Assimilated nitrogen species are initially converted to $NH_3$, which is then incorporated into amino acids from which cellular proteins and chlorophylls are synthesized. Although enzymes converting different nitrogen species to $NH_3$ fractionate nitrogen differently and therefore affect the absolute value of $\delta^{15}N_{cell}$, the isotopic difference between cellular proteins and chlorophylls remains constant within the clade. Accordingly, $\varepsilon_{por}$ is also largely independent of redox conditions during cell growth (15, 46).

The El Mreïti Group porphyrins have $\varepsilon_{por}$ values ranging from −5.1 to −0.5‰ (Table 2). Fig. 6 compares these values with literature data from culture experiments and recent and Phanerozoic sediments. Freshwater cyanobacteria have median $\varepsilon_{por}$ = −10.9‰ (range, −16.0 to −5.7‰; $n$ = 38); marine planktonic cyanobacteria, −0.6‰ (range, −2.9–5.7‰; $n$ = 15); marine benthic cyanobacteria, −10.3‰ (range, −10.4‰ to −10.1‰; $n$ = 2); purple nonsulfur bacteria, +10.1‰ (range, 9.3–15.7‰; $n$ = 3); PSB, +5.8‰ (one environmental sample); and red and green algae, +5.2‰ (range, −0.9–10.1‰; $n$ = 42) (15, 47–53). Particulate organic matter in modern oceans, recent sediments beneath anoxic waters, and Phanerozoic shales all yield positive $\varepsilon_{por}$ values overlapping with the algal signal (Fig. 6), indicating that eukaryotic algae were the dominant export producers in these systems. By contrast, the new Mesoproterozoic $\varepsilon_{por}$ values clearly fall into the range of cyanobacteria. However, the assignment of the Mesoproterozoic $\varepsilon_{por}$ values to cyanobacteria has some remaining uncertainty. Most organism-specific values in Fig. 6 are based on laboratory data from a limited number of species and may not fully reflect natural conditions or variabilities. Moreover, the compilation is missing some groups of phototrophic bacteria that may have been important in the Mesoproterozoic, particularly Chloroflexi and Chlorobiaceae. Thus, the Mesoproterozoic porphyrins probably have a dominant cyanobacterial source plus an unknown contribution from anoxygenic phototrophic bacteria. Notable eukaryotic algal input, however, is unlikely based on the considerable and consistent offset between the positive $\varepsilon_{por}$ of algae-dominated Phanerozoic sediments and the negative $\varepsilon_{por}$ of the Mesoproterozoic porphyrins.

**Hydrocarbon Biomarker Evidence for Primary Producers.** Carotenoid derivatives of the 2,3,4- and 2,3,6-AI series are present in all El Mreïti Group shales (Fig. 2*B*). 2,3,4-AI may be derived from the biological carotenoid derivatives okenane, renieratane, and renierapurpurane, which are all diagnostic for PSB of the family Chromatiaceae (4). The 2,3,6-AI series is most commonly derived from aromatic carotenoids with the cholorobactane, isorenieratane, and/or β-isorenieratane skeletons found in green sulfur bacteria (GSB) (Chlorobiaceae). As 2,3,4- and 2,3,6-AI are abundant in all Taoudeni bitumens, PSB and GSB probably played an important ecological role. While both families produce BChl *a* (54), some PSB also produce BChl *b* (55) and GSB additionally synthesize BChl *c*, *d*, or *e* (*SI Appendix*, Table S2). These BChls would all have contributed to the porphyrin pool of the extracts. However, their impact remains uncertain because

**Table 2. Molecular weight and stable isotope data for individual porphyrins of 13-Ni**

| Peak* | Structure† | [M+] | mV‡ | C/N$_{predicted}$ | C/N$_{measured}$ | $\delta^{15}N_{por}$, ‰ | $\delta^{13}C_{por}$,§ ‰ | $\varepsilon_{por}$,¶ ‰ |
|---|---|---|---|---|---|---|---|---|
| A | $C_{28}$ Etio | 479 | 389 | 7.00 | 18.5 | 7.8 | −28.6 | −2.7 |
| B | $C_{29}$ Etio | 493 | 446 | 7.25 | 16.4 | 7.3 | −28.4 | −2.2 |
| C | $C_{30}$ Etio | 507 | N.A.# | 7.50 | N.A. | N.A. | N.A. | N.A. |
| D | $C_{30}$ DPEP | 505 | 310 | 7.50 | 13.0 | 8.8 | −29.7 | −3.7 |
| E-1 | $C_{31}$ Etio | 521 | 150 | 7.75 | 22.1 | 10.2 | −29.2 | −5.1 |
| E-2 | $C_{31}$ Etio | 521 | 335 | 7.75 | 12.7 | 5.6 | −29.5 | −0.5 |
| F | $C_{32}$ DPEP | 533 | 332 | 8.00 | 14.1 | 7.2 | −27.2 | −2.1 |

N.A., not available.

*Peak identification in HPLC chromatogram and APCI mass spectra are given in *SI Appendix*, Fig. S3.

†Structures tentatively assigned based on molecular weight determined by APCI.

‡Detector response of the elemental analysis–isotope ratio mass spectrometry system (1 mV is equivalent to ~1 ng N). Procedural HPLC blanks yielded N-background values of ~10 mV (*SI Appendix, SI Methods*). The Ni octaethylporphyrin standard was injected in the concentration range of 110–610 mV (nine standard measurements before, middle, and after samples), yielding $\delta^{15}N = +0.86 \pm 0.4‰$, and $\delta^{13}C = -34.17 \pm 0.2‰$. There are no correlations between compound concentration (detector response) and $\delta^{15}N_{por}$ or C/N$_{measured}$.

§Mixed signal of porphyrin and coeluting unknown hydrocarbons (*SI Appendix*).

¶$\varepsilon_{por} = \delta^{15}N_{bulk} - \delta^{15}N_{por} = 5.1‰ - \delta^{15}N_{por}$.

#Peak C in the reversed-phase HPLC chromatogram broke into several smaller peaks during the normal-phase HPLC step, with individual concentrations too low for isotopic measurement.

$\varepsilon_{por}$ is unknown for GSB, and only a single value is available from a lacustrine PSB species ($\varepsilon_{por} = +5.8‰$) (11).

The ratio of eukaryotic steranes over bacterial hopanes (S/H) is a first-order estimate for the relative contribution of eukaryotic to bacterial biomass to sediments. Although hopanes were abundant in the black shales of the El Mreïti Group, steranes remained beneath detection limits. Quantification of background noise shows that steranes, if present, fall below S/H = 0.0002–0.0014 (Table 1), which is one to two orders of magnitude lower than the Tonian average (1,000–720 Ma; S/H = 0.06 ± 0.10), and two to four orders of magnitude lower than typical Ediacaran to Phanerozoic values (635 Ma to present; average S/H = 0.75 ± 1.1) (Fig. 1*A*) (8).

Most molecular clocks estimate the origin of the last common ancestor of all extant eukaryotes (LECA) >1,400 Ma (e.g., ref. 10). LECA possessed all enzymes required to biosynthesize most modern common sterols (56). Thus, the absence of steranes in 1,100 Ma El Mreïti Group shales must be related to preferential heterotrophic degradation of sterols or to an ecological insignificance (or absence) of crown group eukaryotes, particularly eukaryotic algae, during deposition of the black shales. According to the "mat-seal" hypothesis, biomarkers from planktonic algae are generally underrepresented in pre-Ediacaran bitumens due to strong heterotrophic reworking of algal debris on the surface of oxygen-producing, shallow-water microbial mats (14). However, this mechanism cannot apply to the black shales of the Touirist Formation, which formed during maximum flooding of the West African Craton beneath relatively deep, anoxic waters (19). Alternatively, sterols may have suffered severe recycling as planktonic algal debris sank slowly through the water column (14). However, the preservation of cyanobacterial porphyrins also excludes this mechanism. Senescent picoplanktonic cyanobacterial cells sink considerably slower than larger algal cells (57), causing preferential degradation of cyanobacterial over algal porphyrins, a process observed in the modern Black Sea (16). Such preferential degradation of slower sinking bacterial biomass would have elevated, not attenuated, the sterane/hopane ratio. Most importantly, however, porphyrins are degradation sensitive, and their mere existence demonstrates that photosynthetic organic matter suffered little degradation during deposition of the El Mreïti Group shales. Therefore, the lack of detectable steranes is not likely related to severe and selective degradation of algal biomass, but presumably reflects primary paucity of sterol-producing eukaryotes (for further discussion, see *SI Appendix, SI Taphonomic Biases*).

**The Phototrophic Community and the Dominant Primary Producer.** The biomarker assemblage of the 1,100 Ma El Mreïti Group shales suggests that the community of phototrophs included cyanobacteria, PSB, and GSB. Based on the absence of steranes and low $\varepsilon_{por}$ values, eukaryotic algae did not play a detectable role. Although ornamented and process-bearing organic-walled microfossils interpreted as unambiguously eukaryotic are present in El Mreïti Group sediments (58), they do not display evidence of algal affinity. Particularly the process-bearing taxon *Trachyhystrichosphaera aimika* can be locally abundant in subtidal sediments, and its morphology rather suggests osmotrophy, as was proposed for older Mesoproterozoic microfossils (*Tappania*) (59).

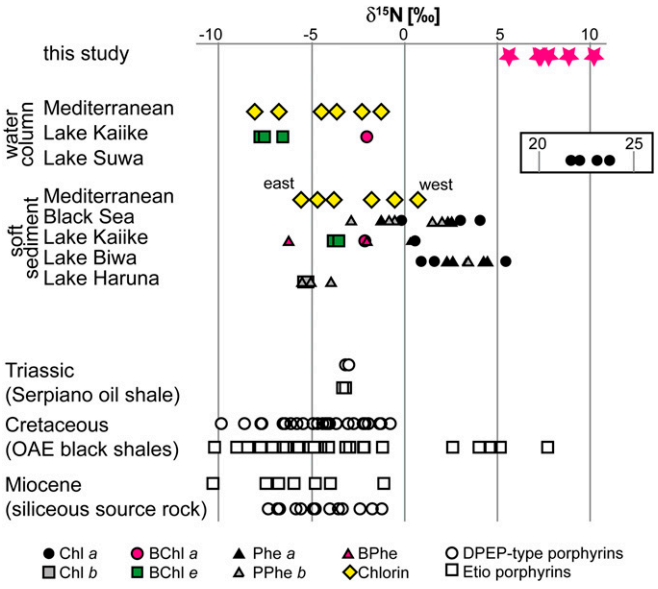


**Fig. 5.** $\delta^{15}N$ values of chlorophylls and porphyrin derivatives from Touirist Formation sample 13-Ni (pink stars), the water column and sediments of various modern water bodies, and Phanerozoic sediments. Lakes, freshwater lakes (compiled from refs. 37, 48, 52, and 75). BPhe, bacteriopheophytin; Phe, pheophytin; PPhe, pyropheophytin.

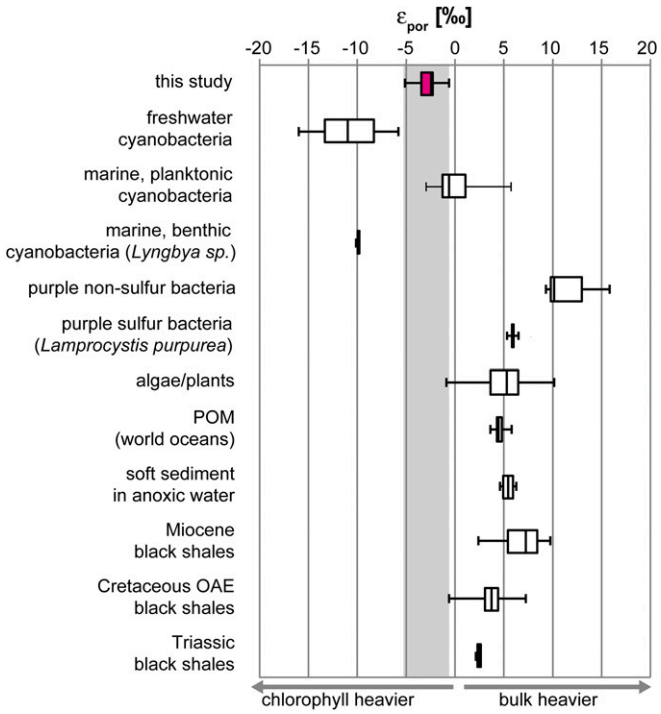


**Fig. 6.** Whisker plot of a wide range of $\varepsilon_{por}$ data (15, 47, 48, 50–53). "This study" is Touirist Formation sample 13-Ni.

However, based on biomarker data, none of these organisms was a quantitatively important contributor of organic matter to black shale facies in the Taoudeni Basin.

The biomarker distribution of the El Mreïti Group shales is typical of the mid-Proterozoic (14). All mid-Proterozoic successions, when analyzed under strict exclusion of contamination, fail to yield diagnostic eukaryotic steranes despite the presence of bacterial hopanes. This includes the 1,640 Ma Barney Creek Formation (5), 1,390 Ma Xiamaling Formation (60), 1,310 Ma Velkerri Formation (14, 61, 62), 1,100 Ma Nonesuch Formation (14), and 1,000 Ma Lakhanda and Ui groups (14) (Fig. 1*A*). Absence or low activity of eukaryotic algae thus appears to be a common attribute of mid-Proterozoic open water environments wherever biomarkers are preserved.

The mid-Proterozoic biomarker compositions are a strong contrast to younger assemblages. 900–800 Ma, the first clearly indigenous, diagnostic eukaryotic steranes emerge (6, 7) followed by a permanent transition from dominantly bacterial to eukaryotic export production 659–645 Ma (Fig. 1) (8). After 645 Ma, steranes are almost always present in marine ecosystems (8) and the N-isotopic composition of Phanerozoic porphyrins indicates a persistent dominance of algal over cyanobacterial carbon burial, even during Oceanic Anoxic Events (Fig. 6) (50).

The incumbency of bacteria through the mid-Proterozoic and the perceived late transition to a more eukaryotic world is one of the most intriguing, yet unresolved, phenomena of Precambrian biology. Explanations may include sulfide poisoning of eukaryotes in euxinic Proterozoic basin margins (63, 64) and severe paucity of biolimiting nutrients such as nitrogen (63) and phosphate (8, 65). However, Proterozoic marine environments, including the Taoudeni Basin (19), were largely ferruginous rather than sulfidic (66), and nutrient limitation scenarios are hard to maintain for depositional environments with extremely carbon-rich sediments such as the black shales of the 1,100 Ma El Mreïti Group and 1,390 Ma Xiamaling Formation (67) with organic carbon contents >30%. Such shales likely formed beneath nutrient-replete waters (67) and not during conditions of severe nitrate or phosphate limitation (57). The exclusion of algal cells in areas of high nutrient flow is hard to explain, even in the absence of grazing pressure (2). Thus, adequate explanations for the prevalence of bacterial phytoplankton may require addition of self-sustaining ecological feedback loops, such as the shading effect of dense planktonic cyanobacterial populations, which may exclude algae with higher light requirements (57).

While the paucity of planktonic algae in the mid-Proterozoic remains enigmatic, the persistence of bacterial phytoplankton has profound ecological and evolutionary consequences. In the water column of most mid-Proterozoic marine environments, slow-sinking bacterial plankton was presumably recycled within the microbial loop, leading to diminished transport of nutrients to the deep ocean and upwelling zones, and a reduced flux of organic carbon to bottom sediments (57). As permanent burial of reduced carbon is offset by a net release of molecular oxygen into the atmosphere, the sinking behavior of bacterial phytoplankton may thus have contributed to mid-Proterozoic atmospheric oxygen levels significantly lower than at present. Low atmospheric oxygen concentration and the aerobic degradation of bacterial biomass within the water column may have contributed to the pervasively anoxic nature of mid-Proterozoic marine basins (64, 68–70).

In modern oceans, relatively large eukaryotic phytoplankton cells create food webs with efficient nutrient and energy transfers to higher trophic levels, fueling the proliferation of orders-of-magnitude larger grazers and predators (2, 71). By contrast, in mid-Proterozoic pelagic environments with phototrophic bacteria at the base of the food web, a large proportion of carbon and energy may have been lost within the microbial loop. Based on the fossil record (58), such trophic systems may only have sustained relatively small protists at their apex. In combination with low atmospheric oxygen levels (68, 69, 72) and unstable redox conditions (73), the inefficient flow of energy from the base of the mid-Proterozoic food web to higher trophic levels may have inhibited the evolution of complex eukaryotic ecosystems and large, animal-like organisms.

## Materials and Methods

Extended methods are available in *SI Appendix, SI Methods*. Briefly, biomarker analysis was performed at the Australian National University (ANU) under standard operational procedures and included a thorough syngeneity assessment (20–22). Hydrocarbons were analyzed on a Waters AutoSpec Premier double-sector mass spectrometer interfaced with a 6890 GC (Agilent), fitted with a DB-5MS capillary column. Porphyrin determination using reversed-phase HPLC-UV/Vis followed the standard operating procedure, and used the porphyrin injection standards of Geoscience Australia (Canberra) (24, 25), and was conducted at the ANU using an Agilent 1100 system containing a degasser (G1379A, JP 40714), a Quat Pump (G1311A, DE 40926343214), and a DAD (G1315B, DE40521369). Molecular characterization of porphyrins was performed at the National High Magnetic Field Laboratories in Tallahassee, Florida (26), using a 9.4-tesla FT-ICR mass spectrometer. For bulk analyses, ~250 μg of total organic matter of decalcified rock powder was weighed into a tin capsule with 4 mg of vanadyl oxide ($VO_2O_5$, Alfa Aesar, 99.6%) and the bulk N and C content as well as their isotopic composition were measured using a Sercon 20–22 IRMS connected to an ANCA-GSL CHN elemental analyzer. The average SD measured on samples was 0.06‰. Compound-specific isotope analyses on Ni-porphyrins were performed at JAMSTEC (Japan) following the methods of Ogawa et al. (74).

**ACKNOWLEDGMENTS.** We thank L. Krajewski for FT-ICR MS measurements, H. Suga and N. O. Ogawa at JAMSTEC for purification and measurement of isotopic compositions of individual porphyrins, and J. Hope for technical assistance at ANU. This work was supported in part by Australian Research Council Grants DP1095247 and DP160100607 (to J.J.B.) and by Belgian Science Policy Interuniversity Attraction Pole "PLANET TOPERS" and European Research Council Starting Grant ELiTE FP7/308074 (to E.J.J. and J.B.). A portion of the work was performed at the National High Magnetic Field Laboratory at Florida State University, which is supported by the National Science Foundation through Grant DMR 11-57490 and the State of Florida. C.J.B. publishes with the permission of the chief executive officer of Geoscience Australia.

1. Knoll AH, Summons R, Waldbauer JR, Zumberge JE (2007) The geological succession of primary producers in the oceans. *The Evolution of Primary Producers in the Sea*, eds Falkowski P, Knoll AH (Elsevier, Burlington, MA), pp 133–163.
2. Irwin AJ, Finkel ZV, Schofield OME, Falkowski PG (2006) Scaling-up from nutrient physiology to the size-structure of phytoplankton communities. *J Plankton Res* 28: 459–471.
3. Butterfield NJ (2015) Proterozoic photosynthesis—a critical review. *Palaeontology* 58: 953–972.
4. Brocks JJ, Schaeffer P (2008) Okenane, a biomarker for purple sulfur bacteria (Chromatiaceae), and other new carotenoid derivatives from the 1,640 Ma Barney Creek Formation. *Geochim Cosmochim Acta* 72:1396–1414.
5. Brocks JJ, et al. (2005) Biomarker evidence for green and purple sulphur bacteria in a stratified Palaeoproterozoic sea. *Nature* 437:866–870.
6. Brocks JJ, et al. (2016) Early sponges and toxic protists: Possible sources of cryostane, an age diagnostic biomarker antedating Sturtian snowball Earth. *Geobiology* 14: 129–149.
7. Hoshino Y, et al. (2017) Cryogenian evolution of stigmasteroid biosynthesis. *Sci Adv* 3: e1700887.
8. Brocks JJ, et al. (2017) The rise of algae in Cryogenian oceans and the emergence of animals. *Nature* 548:578–581.
9. Summons RE, et al. (1988) Distinctive hydrocarbon biomarkers from fossiliferous sediments of the late Proterozoic Walcott member, Chuar group, Grand Canyon, Arizona. *Geochim Cosmochim Acta* 52:2625–2637.
10. Parfrey LW, Lahr DJG, Knoll AH, Katz LA (2011) Estimating the timing of early eukaryotic diversification with multigene molecular clocks. *Proc Natl Acad Sci USA* 108: 13624–13629.
11. Sánchez-Baracaldo P, Raven JA, Pisani D, Knoll AH (2017) Early photosynthetic eukaryotes inhabited low-salinity habitats. *Proc Natl Acad Sci USA* 114:E7737–E7745.
12. Gibson TM, et al. (2017) Precise age of *Bangiomorpha pubescens* dates the origin of eukaryotic photosynthesis. *Geology* 46:135–138.
13. Butterfield NJ, Knoll AH, Swett K (1990) A bangiophyte red alga from the Proterozoic of arctic Canada. *Science* 250:104–107.
14. Pawlowska MM, Butterfield NJ, Brocks JJ (2013) Lipid taphonomy in the Proterozoic and the effect of microbial mats on biomarker preservation. *Geology* 41:103–106.
15. Higgins MB, et al. (2011) Paleoenvironmental implications of taxonomic variation among $\delta^{15}$N values of chloropigments. *Geochim Cosmochim Acta* 75:7351–7363.
16. Fulton JM, Arthur MA, Freeman KH (2012) Black Sea nitrogen cycling and the preservation of phytoplankton $\delta^{15}$N signals during the Holocene. *Global Biogeochem Cycles* 26:GB2030.
17. Rooney AD, Selby D, Houzay J-P, Renne PR (2010) Re–Os geochronology of a Mesoproterozoic sedimentary succession, Taoudeni basin, Mauritania: Implications for basin-wide correlations and Re–Os organic-rich sediments systematics. *Earth Planet Sci Lett* 289:486–496.
18. Kah LC, Bartley JK, Teal DA (2012) Chemostratigraphy of the late Mesoproterozoic Atar group, Taoudeni Basin, Mauritania: Muted isotopic variability, facies correlation, and global isotopic trends. *Precambrian Res* 200–203:82–103.
19. Beghin J, et al. (2017) A palaeoecological model for the late Mesoproterozoic–early Neoproterozoic Atar/El Mreïti group, Taoudeni Basin, Mauritania, northwestern Africa. *Precambrian Res* 299:1–14.
20. Brocks JJ (2011) Millimeter-scale concentration gradients of hydrocarbons in Archean shales: Live-oil escape or fingerprint of contamination? *Geochim Cosmochim Acta* 75: 3196–3213.
21. Schinteie R, Brocks JJ (2014) Evidence for ancient halophiles? Testing biomarker syngeneity of evaporites from Neoproterozoic and Cambrian strata. *Org Geochem* 72: 46–58.
22. Jarrett A, Schinteie R, Hope JM, Brocks JJ (2013) Micro-ablation, a new technique to remove drilling fluids and other contaminants from fragmented and fissile rock material. *Org Geochem* 61:57–65.
23. Blumenberg M, Thiel V, Riegel W, Kah LC, Reitner J (2012) Biomarkers of black shales formed by microbial mats, late Mesoproterozoic (1.1 Ga) Taoudeni Basin, Mauritania. *Precambrian Res* 196–197:113–127.
24. Boreham CJ, Fookes CJ (1989) Separation of nickel (II) alkylporphyrins by reversed-phase high-performance liquid chromatography: Methodology and application. *J Chromatogr A* 467:195–208.
25. Boreham CJ (1992) Reversed-phase high-performance liquid chromatography of metalloporphyrins. *Biological Markers in Sediments and Petroleum*, eds Moldowan JM, Albrecht P, Philp RP (Prentice-Hall, Englewood Cliffs, NJ), pp 301–312.
26. McKenna AM, Purcell JM, Rodgers RP, Marshall AG (2009) Identification of vanadyl porphyrins in a heavy crude oil and raw asphaltene by atmospheric pressure photoionization Fourier transform ion cyclotron resonance (FT-ICR) mass spectrometry. *Energy Fuels* 23:2122–2128.
27. Eckardt C, et al. (1991) Preservation of chlorophyll-derived pigments in sedimentary organic matter. *Philos Trans R Soc Lond B Biol Sci* 333:339–348.
28. Stüeken EE (2013) A test of the nitrogen-limitation hypothesis for retarded eukaryote radiation: Nitrogen isotopes across a Mesoproterozoic basinal profile. *Geochim Cosmochim Acta* 120:121–139.
29. Robinson RS, et al. (2012) A review of nitrogen isotopic alteration in marine sediments. *Paleoceanography*, 27:PA4203.
30. Calvert SE (2004) Beware intercepts: Interpreting compositional ratios in multicomponent sediments and sedimentary rocks. *Org Geochem* 35:981–987.
31. Williams LB, Ferrell RE (1991) Ammonium substitution in illite during maturation of organic matter. *Clays Clay Miner* 39:400–408.
32. Thomazo C, Ader M, Philippot P (2011) Extreme $^{15}$N-enrichments in 2.72-Gyr-old sediments: Evidence for a turning point in the nitrogen cycle. *Geobiology* 9:107–120.
33. Ader M, et al. (2016) Interpretation of the nitrogen isotopic composition of Precambrian sedimentary rocks: Assumptions and perspectives. *Chem Geol* 429:93–110.
34. Lehmann MF, Bernasconi SM, Barbieri A, McKenzie JA (2002) Preservation of organic matter and alteration of its carbon and nitrogen isotope composition during simulated and in situ early sedimentary diagenesis. *Geochim Cosmochim Acta* 66: 3573–3584.
35. Çoban-Yıldız Y, Altabet MA, Yılmaz A, Tuğrul S (2006) Carbon and nitrogen isotopic ratios of suspended particulate organic matter (SPOM) in the Black Sea water column. *Deep Sea Res Part II Top Stud Oceanogr* 53:1875–1892.
36. Fry B, et al. (1991) Stable isotope studies of the carbon, nitrogen and sulfur cycles in the Black Sea and the Cariaco Trench. *Deep-Sea Res Part A* 38:S1003–S1019.
37. Ohkouchi N, Takano Y (2013) Organic nitrogen: Sources, fates, and chemistry. *Treatise in Geochemistry* (Elsevier, Amsterdam), 2nd Ed, pp 1–38.
38. Sundararaman P, Dahl JE (1993) Depositional environment, thermal maturity and irradiation effects on porphyrin distribution: Alum Shale, Sweden. *Org Geochem* 20: 333–337.
39. Callot HJ, Ocampo R (2000) *Geochemistry of Porphyrins the Porphyrin Handbook: Synthesis and Organic Chemistry*, eds Kadish KM, Smith KM, Guilard R (Academic, San Diego), Vol 1, p 349.
40. Chicarelli M, Wolff G, Murray M, Maxwell J (1984) Porphyrins with a novel exocyclic ring system in an oil shale. *Tetrahedron* 40:4033–4039.
41. Verne-Mismer J, Ocampo R, Callot HJ, Albrecht P (1990) New chlorophyll fossils from Moroccan oil shales. Porphyrins derived from chlorophyll $C_3$ or a related pigment? *Tetrahedron Lett* 31:1751–1754.
42. Verne-Mismer J, Ocampo R, Callot H, Albrecht P (1988) Molecular fossils of chlorophyll *c* of the 17-nor-DPEP Series. Structure determination, synthesis, geochemical significance. *Tetrahedron Lett* 29:371–374.
43. Chen M, Hiller RG, Howe CJ, Larkum AW (2005) Unique origin and lateral transfer of prokaryotic chlorophyll-*b* and chlorophyll-*d* light-harvesting systems. *Mol Biol Evol* 22:21–28.
44. Ito H, Ohtsuka T, Tanaka A (1996) Conversion of chlorophyll *b* to chlorophyll *a* via 7-hydroxymethyl chlorophyll. *J Biol Chem* 271:1475–1479.
45. Zapata M, Garrido JL, Jeffrey SW (2006) Chlorophyll *c* pigments: Current status. *Chlorophylls and Bacteriochlorophylls: Biochemistry, Biophysics, Functions and Applications*, eds Grimm B, Porra RJ, Rüdiger W, Scheer H (Springer Netherlands, Dordrecht, The Netherlands), pp 39–53.
46. Waser N, Harrison P, Nielsen B, Calvert S, Turpin D (1998) Nitrogen isotope fractionation during the uptake and assimilation of nitrate, nitrite, ammonium, and urea by a marine diatom. *Limnol Oceanogr* 43:215–224.
47. Asahina K, et al. (2010) The first experimental demonstration of side chain extension of geoporphyrins in sediments. *Chem Lett* 39:1267–1269.
48. Kashiyama Y, et al. (2008) Diazotrophic cyanobacteria as the major photoautotrophs during mid-Cretaceous oceanic anoxic events: Nitrogen and carbon isotopic evidence from sedimentary porphyrin. *Org Geochem* 39:532–549.
49. Sachs JP, Repeta DJ, Goericke R (1999) Nitrogen and carbon isotopic ratios of chlorophyll from marine phytoplankton. *Geochim Cosmochim Acta* 63:1431–1441.
50. Higgins MB, Robinson RS, Husson JM, Carter SJ, Pearson A (2012) Dominant eukaryotic export production during ocean anoxic events reflects the importance of recycled $NH_4^+$. *Proc Natl Acad Sci USA* 109:2269–2274.
51. Higgins MB, Robinson RS, Carter SJ, Pearson A (2010) Evidence from chlorin nitrogen isotopes for alternating nutrient regimes in the Eastern Mediterranean Sea. *Earth Planet Sci Lett* 290:102–107.
52. Chicarelli MI, Hayes JM, Popp BN, Eckardt CB, Maxwell JR (1993) Carbon and nitrogen isotopic compositions of alkyl porphyrins from the triassic serpiano oil shale. *Geochim Cosmochim Acta* 57:1307–1311.
53. Ohkouchi N, Kashiyama Y, Kuroda J, Ogawa N, Kitazato H (2006) The importance of diazotrophic cyanobacteria as primary producers during Cretaceous Oceanic Anoxic Event 2. *Biogeosciences* 3:467–478.
54. Scheer H (2006) An overview of chlorophylls and bacteriochlorophylls: biochemistry, biophysics, functions and applications. *Chlorophylls and Bacteriochlorophylls* (Springer, Dordrecht, The Netherlands), pp 1–26.
55. Imhoff JF (2006) The Chromatiaceae. *Prokaryotes*, eds Dworkin M, Falkow S, Rosenberg E, Schleifer K-H, Stackebrandt E (Springer, New York), Vol 7, pp 846–873.
56. Desmond E, Gribaldo S (2009) Phylogenomics of sterol synthesis: Insights into the origin, evolution, and diversity of a key eukaryotic feature. *Genome Biol Evol* 1: 364–381.
57. Butterfield NJ (2009) Macroevolutionary turnover through the Ediacaran transition: Ecological and biogeochemical implications. *Geol Soc Lond Spec Publ* 326:55–66.
58. Beghin J, et al. (2017) Microfossils from the late Mesoproterozoic–early Neoproterozoic Atar/El Mreïti group, Taoudeni Basin, Mauritania, northwestern Africa. *Precambrian Res* 291:63–82.
59. Javaux E, Knoll A (2017) Micropaleontology of the lower Mesoproterozoic Roper group, Australia, and implications for early eukaryotic evolution. *J Paleontol* 91: 199–229.
60. Luo G, Hallmann C, Xie S, Ruan X, Summons RE (2015) Comparative microbial diversity and redox environments of black shale and stromatolite facies in the Mesoproterozoic Xiamaling Formation. *Geochim Cosmochim Acta* 151:150–167.
61. Flannery EN, George SC (2014) Assessing the syngeneity and indigeneity of hydrocarbons in the ~1.4 Ga Velkerri Formation, McArthur Basin, using slice experiments. *Org Geochem* 77:115–125.
62. Yang B, et al. (2018) Spatial and temporal variation in detrital zircon age provenance of the hydrocarbon-bearing upper Roper group, Beetaloo sub-basin, Northern Territory, Australia. *Precambrian Res* 304:140–155.
63. Anbar AD, Knoll AH (2002) Proterozoic ocean chemistry and evolution: A bioinorganic bridge? *Science* 297:1137–1142.

64. Poulton SW, Fralick PW, Canfield DE (2010) Spatial variability in oceanic redox structure 1.8 billion years ago. *Nat Geosci* 3:486–490.
65. Reinhard CT, et al. (2017) Evolution of the global phosphorus cycle. *Nature* 541:386–389.
66. Planavsky NJ, et al. (2011) Widespread iron-rich conditions in the mid-Proterozoic ocean. *Nature* 477:448–451.
67. Zhang S, et al. (2016) Sufficient oxygen for animal respiration 1,400 million years ago. *Proc Natl Acad Sci USA* 113:1731–1736.
68. Canfield DE (2014) *Oxygen—A Four Billion Year History* (Princeton Univ Press, Princeton).
69. Planavsky NJ, et al. (2014) Earth history. Low mid-Proterozoic atmospheric oxygen levels and the delayed rise of animals. *Science* 346:635–638.
70. Lyons TW, Reinhard CT, Planavsky NJ (2014) The rise of oxygen in Earth's early ocean and atmosphere. *Nature* 506:307–315.
71. Knoll AH, Follows MJ (2016) A bottom-up perspective on ecosystem change in Mesozoic oceans. *Proc Biol Sci* 283:20161755.
72. Reinhard CT, Planavsky NJ, Olson SL, Lyons TW, Erwin DH (2016) Earth's oxygen cycle and the evolution of animal life. *Proc Natl Acad Sci USA* 113:8933–8938.
73. Johnston DT, et al. (2012) Late Ediacaran redox stability and metazoan evolution. *Earth Planet Sci Lett* 335–336:25–35.
74. Ogawa N, Nagata T, Kitazato H, Ohkouchi N (2010) Ultra sensitive elemental analyzer/isotope ratio mass spectrometer for stable nitrogen and carbon isotope analyses. *Earth, Life and Isotopes* (Kyoto Univ Press, Kyoto), pp 339–353.
75. Kashiyama Y, Ogawa N, Nomoto S, Kitazato H, Ohkouchi N (2010) Nitrogen and carbon isotopic compositions of copper, nickel, and vanadyl porphyrins in Cretaceous black shales. *Earth, Life, and Isotopes* (Kyoto Univ Press, Kyoto), pp 313–335.